Optimization of chemical vapor deposited (CVD) graphene transfer for nanopore devices

Telma Daniela Azevedo da Silva Oliveira

December 2015

Abstract

Nanopores are nanometer scaled holes in an impermeable membrane and have been studied with the purpose of sequencing DNA. DNA entering and exiting the pore causes dips in the ionic current, providing a signal from which the DNA sequence could potentially be obtained. A graphene membrane opens up the possibility of single nucleotide detection, due to its single-atom thickness. CVD graphene has been studied as an alternative to exfoliated graphene because of its large carbon monolayer which has many advantages to the small graphene flakes obtained by exfoliation, which are difficult to produce. To be used in nanopore membranes, CVD graphene has to be transferred from the metal substrate in which it was grown to the desired substrate. This is frequently accomplished using a polymer support to transfer the graphene to the measuring device. However, breaks and polymer residues are frequently found in the membrane. The impact of transfer parameters on graphene morphology and structure was studied. Optical microscopy and atomic force microscopy showed that addition of a baking step after PMMA spin coating lead to improvements in particle density and roughness parameters. Similar results were obtained by addition of a baking step after graphene/PMMA films transfer to the final substrate. Longer deionized water steps during hydrochloric acid cleaning also reduced particle density and roughness was improved. Also, annealing the samples at high temperatures highly reduced PMMA residue density.

Keywords: nanopores, graphene, chemical vapor deposition, PMMA transfer method, atomic force microscopy

1. Introduction

Knowledge of DNA sequences of different organisms contributed to significant advances in biological research, leading to major breakthroughs in the fields of medicine and biotechnology [1]. In the last decade, nanopore based devices have been subject of substantial research for the purpose of sequencing DNA.

The principle behind nanopores is that a nanoscale hole is made in an impermeable membrane. Voltage application across the pore will cause ion migration, leading to electric current that will be measured. Transient changes in the ionic current can be associated with pore occupation by a macromolecule, therefore, the translocation of a molecule through a pore can be sensed by these changes [2].

Silicon-based membranes have been studied for nanopore applications, however their thickness corresponds to 60 DNA bases along a single stranded DNA molecule. On the other hand, graphene, being 0,3 nm thick (the thickness a single atomic layer), opens the possibility of single base detection of DNA [3].

Graphene sheets are usually obtained by graphene exfoliation, however single layer graphene sheets are quite rare and small [4]. With CVD (chemical vapor deposited) graphene, which is produced by decomposition of carbon compounds on a metal surface, it is possible to obtain large areas of monolayer graphene. However, this technique requires the removal of the metal and a transfer process, which may cause the graphene to deteriorate [5]. .

The experimental part of this project was carried out in the Kavli Nanolab Delft facilities, under the supervision of MSc. Stephanie Heerema and Prof. Dr. Cees Dekker from the Bionanoscience Department in TU Delft.

2. Graphene synthesis by CVD

The principle behind chemical vapor deposition is that the substrate is exposed to gaseous precursors, which when in contact with the substrate at high temperatures, deposit on its surface, creating a thin film [6]. The quality of the materials obtained by CVD is strongly dependent on the process parameters such as gas temperature, pressure, and time duration. To achieve single layer graphene by CVD, with quality similar to exfoliated graphene, these parameters have to be adjusted to the depo-

sition process. [7, 8].

2.1. Kinetics of graphene growth

The process of the CVD graphene film formation consists of four major steps: heating, annealing, growth and cooling. The process occurs inside a CVD chamber, and starts with substrate heating to 1000 °C to boost the pyrolysis (thermochemical decomposition of an organic material at elevated temperatures [9]) of the precursor hydrocarbons gas, usually methane or propane. Afterwards, the elevated temperature promotes the formation of larger grain sizes and smoother surfaces. The third step consists of the pyrolysis of the precursor gas that is added into the chamber. Finally, the gas supply is closed and the chamber is cooled down to room temperature [7].

LPCVD (CVD performed at low pressure) and UHV (ultra high vaccum conditions) favor the growth of uniform and defect free single layer graphene. On the other hand, under atmospheric pressure (APCVD), graphene growth is not non-uniform. [10].

2.2. Graphene nucleation

It is in the first stages of growth that the kinetic factors have a fundamental role on graphene structure. After pyrolysis of the precursor gas, usually methane, carbon species aggregate in the metal surface forming several carbon nuclei, that will grow with time, and eventually meet, forming boundaries. These boundaries are associated with structural defects, degrading significantly graphene quality. Defect density decrease is obtained by producing graphene with bigger domains and less nuclei [11].

To grow continuous graphene with larger domain size a two-step methodology has been pursued. First, nuclei are formed in high temperatures at low methane flow rate and low methane parcial pressure. Subsequently, methane flow rate and pressure is increased to obtain full coverage [12].

3. Graphene Transfer methods

To be used in electronics devices, graphene deposited in a metal substrate has to be transfered to the desired substrate. Not only the growth process influences graphene quality, but also the transfer methods, since graphene quality can deteriorate during the transfer. This process involves the use of a support layer, such as PMMA or PDMS, leading to residue accumulation on the graphene layer. Also, wet etchants, such as ferric chloride ($FeCl_3$), ferric nitrate ($Fe(NO_3)_3$) and ammonium persulfate ($(NH_4S_2O_8)$), are used to remove the metal substrate such as nickel or copper, however besides leaving residues on the graphene it can also break and ripple this layer [13].

3.1. Polymer supported transfer

A possible approach to graphene transfer requires the use of a supporting layer. Since graphene is a single atomic layer of carbon atoms, a support would protect and strengthen it. A successful transfer requires the use of a support layer that does not damage the graphene and, that is resistant to the wet etchant [13].

PDMS (polydimethylsiloxane)

PDMS is a polymer material widely used, not only in soft lithography, but also for graphene transfers. This polymer is robust, moldable and resistant to a variety of etchants. It has a low surface adhesion force, facilitating the PDMS detachment from graphene transfered to the desired substrate [14]. Since PDMS is weakly bounded to the target substrate, but adheres strongly to graphene, it is suitable for the transfer process. [15]. To obtain patterned for device making applications, prepatterned graphene and PDMS moulds have been used [7].

PMMA (poly(methyl methacrylate))

PMMA is the most widely used polymer for CVD graphene transfer [8]. PMMA covalently bounds to graphene, providing a better support for the carbon layer, leading to less cracking and rippling than PDMS. However, since the bounds between PMMA and graphene are stronger, it is more difficult to remove the polymer layer [16].

To improve the quality of the PMMA transfer and avoid degradation, various adjustments have been performed. Although, with PMMA is possible to obtain a graphene layer with improved continuity (if compared to PDMS transfers), some breaks and wrinkles still occur, specially in monolayer graphene. They are caused by wrinkles and other defects that appeared in copper during the CVD growth process [17]. A second PMMA layer approach has also been studied to reduce the breaking, rupturing and wrinkling of the graphene membrane. Improvements in transfer quality have been reported by adding an additional PMMA layer to dissolute the first one[18]. Graphene annealing has also been performed to improve graphene quality [19].

3.2. Transfer-free graphene growth & polymer-free transfer

The main issue with transferring CVD graphene with polymer supports is residue accumulation, membrane rupturing and overall graphene quality deterioration. Growing graphene directly on the substrate would prevent the formation of the irregularities caused by the transfer process. Also, a technique has been developed that consists of placing graphene grown on copper in a metal

etchant solution to remove the copper. to pump out the etchant and pump in IPA to clean copper residues from the graphene [20].

4. Experimental methods

4.1. Standard PMMA transfer

The standard PMMA transfer starts by spin coating an A6 PMMA layer on a 5×5 mm graphene deposited on copper piece (4000 rpm, 1 min, for a 500 μm thickness), followed by cleaning the backside of the copper foil with a small amount of acetone in a cotton wipe, to remove PMMA residues accumulated during spin coating. The PMMA cure was made at room temperature during 10 minutes. To remove the graphene from the backside of the copper foil, the stack is plasma etched for 10 seconds (oxygen flow: 200ml/min, power: 50W). In order to etch the copper foil, the PMMA/graphene/copper/graphene films were immersed on Sigma Aldrich copper etchant for 5 hours or in Transcene CE-100 for 2 hours. After the copper is completely removed, the PMMA/graphene films are transfered to a 1:10 mixed solution of HCl during 20 minutes and then 3 times to DI (deionized) water, during 20 minutes each time. After HCl cleaning, the films are transfered to a Si/SiO_2 wafer and dried in air for 2 hours. Finally, to remove the PMMA, the PMMA/graphene/Si/SiO_2 stack is placed in a acetone bath for 10 minutes. The Si/SiO_2 wafers were previously plasma cleaned in an oxygen flow of 200 ml/min, 500W during 1 minute. Schematics of the process is represented in the image from figure 1.

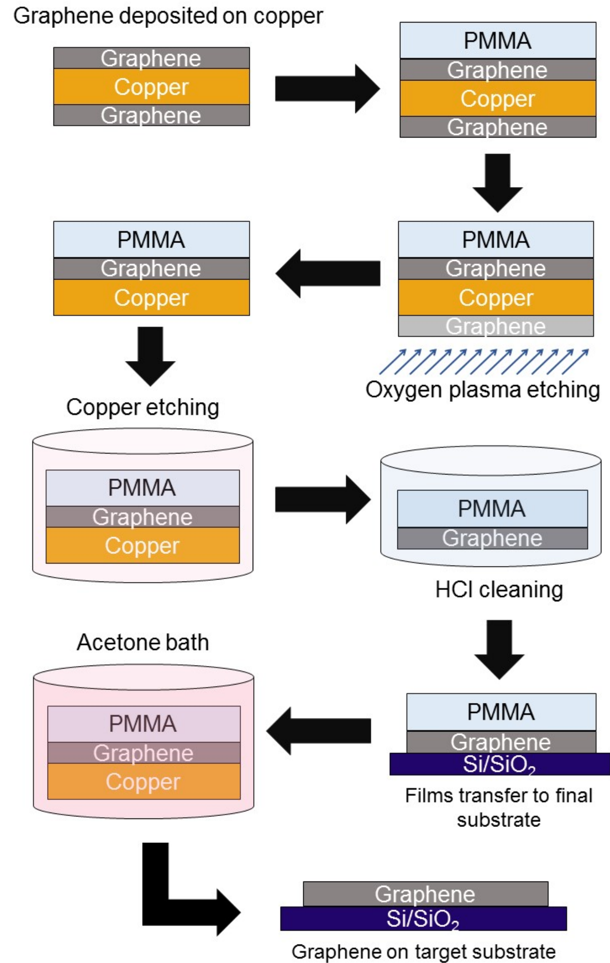

Figure 1: Fundamental steps of CVD graphene transfer by the PMMA method.

5. Results

To optimize CVD graphene transfer into a substrate, the effect of modifications in the standard process described in section 4.1 and in image 1 was studied. Both particle and roughness analysis were carried out, to understand the effect of the modifications in the amount of PMMA residues in the surface and the amount of breaks and wrinkles. Particle analysis and roughness studies were conducted both on the entire AFM images and on $1 \times 1 \mu m^2$ sections of those images. Also, optical microscope images were obtained.

5.1. Standard PMMA transfer

A study was carried out on a standard PMMA CVD graphene transfer batch, which was obtained by the process described on section 4.1 and in image 1. AFM and optical microscope images obtained from these batches can be observed in figure 2 and 3. The success rate (rate of transfers in which the graphene is not visibly damaged) of these transfers is around 50%.

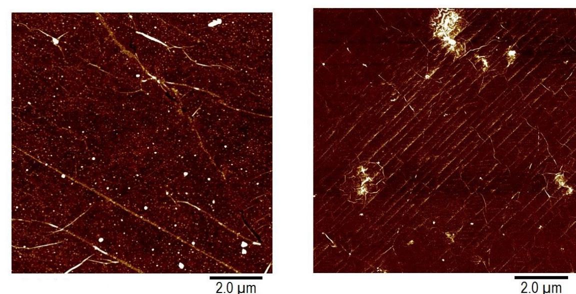

Figure 2: AFM images of CVD graphene transfered by the standard PMMA method.

5.2. Transfer with additional HCl cleaning steps

A study was carried out on a PMMA CVD graphene transfer batch similar to the standard PMMA transfer, except in the HCl cleaning step. The cleaning steps were altered to 20 min in each beaker: 2 times (20 min each time) in DI water and then one

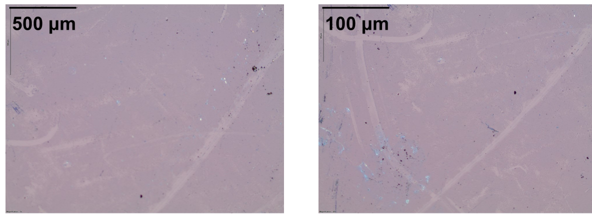

Figure 3: Optical microscope images of CVD graphene transfered by the standard PMMA method, with different magnifications.

time in HCl and finally 3 times in DI water (20 min each time). AFM and optical microscope images obtained from these batches can be observed in figure 4 and 5. The success rate of these transfers was 30%.

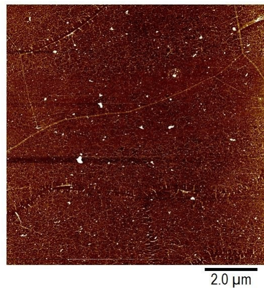

Figure 4: AFM images of CVD graphene transfer carried out with modified HCl cleaning step.

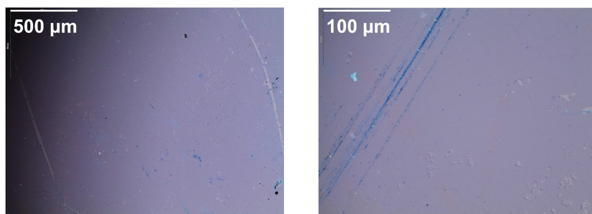

Figure 5: Optical microscope images of CVD graphene transfer carried out with modified HCl cleaning step, with different magnifications.

5.3. Double PMMA layer transfer

A study was carried out on a PMMA CVD graphene transfer batch similar to the standard PMMA transfer, except that, after the first A6 950 K PMMA layer was spin coated (and the polymer was cured in air for 10 minutes), a droplet of A3 950K PMMA was added and cured in air for 2 hours. AFM and optical microscope images obtained from these batches can be seen in figure 6 and 7. The success rate of these transfers was 30%.

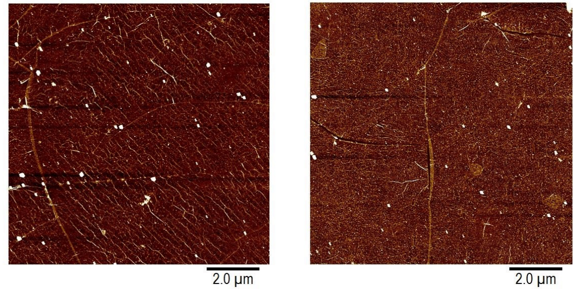

Figure 6: AFM images of CVD graphene transfer carried out with a double PMMA layer.

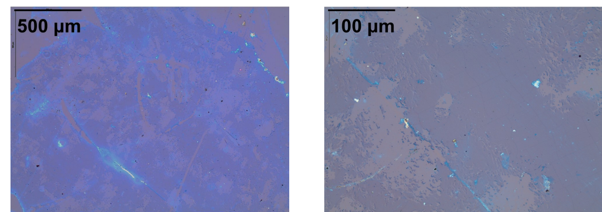

Figure 7: Optical microscope images of CVD graphene transfer carried out with a double PMMA layer, with different magnifications.

5.4. Addition of a baking step after spin coating

A study was carried out on a PMMA CVD graphene transfer batch similar to the standard PMMA transfer, except that, after spin coating, the samples graphene/PMMA films were baked for 5 min at 80°C and then at 130°C for 20 min. AFM and optical microscope images obtained from these batches can be observed in figure 8 and 9. The success rate of these transfers was 90%.

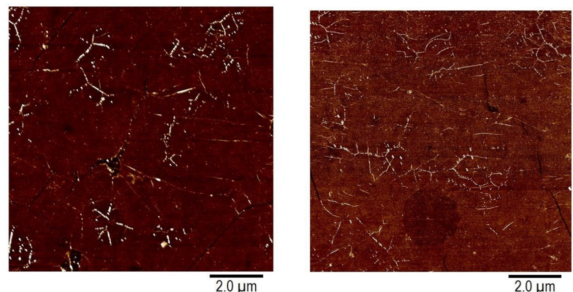

Figure 8: AFM images of CVD graphene transfer with an additional baking step after spin coating.

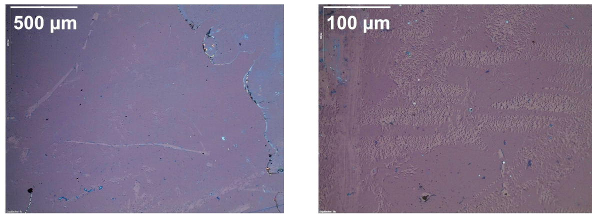

Figure 9: Optical microscope images of CVD graphene transfer carried outwith an additional baking step after spin coating, with different magnifications.

5.5. Addition of a baking step after transfer to substrate

A study was carried out on a PMMA CVD graphene transfer batch similar to the standard PMMA transfer, except that, after HCl cleaning and transfer of PMMA/graphene/copper/substrate, the samples were baked for 5 min at 80°C and then 20 min at 130°C. AFM and optical microscope images obtained from these batches can be seen in figure 10 and 11. The success rate of these transfers was 90%.

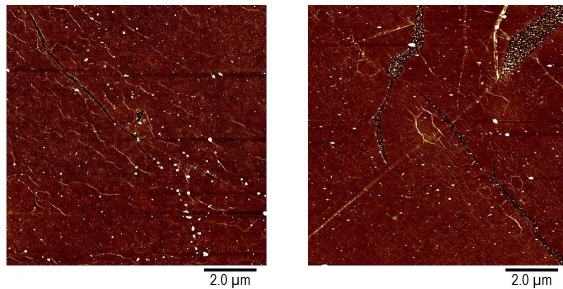

Figure 10: AFM images of CVD graphene transfer with a baking step after transfer to substrate.

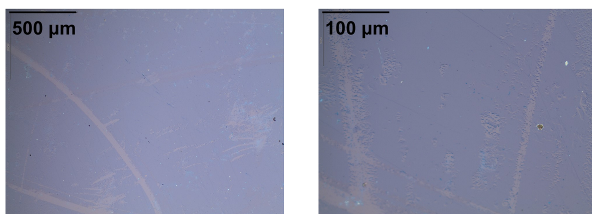

Figure 11: Optical microscope images of CVD graphene transfer with a baking step after transfer to substrate, with different magnifications.

5.6. Addition of a baking step after transfer to substrate and annealing

A study was carried out on a PMMA CVD graphene transfer batch, similar to the standard PMMA transfer, except that, after HCl cleaning and transfer of PMMA/graphene/copper/substrate, the samples were baked for 5 min at 80 °C and then 20 min at 130 °C. Thus, after the acetone bath the samples were annealed for 2 hours at 500 °C with a forming gas flow of hydrogen and argon. AFM and optical microscope images obtained from these batches can be seen in figure 12 and 13. The success rate of these transfers was 90%.

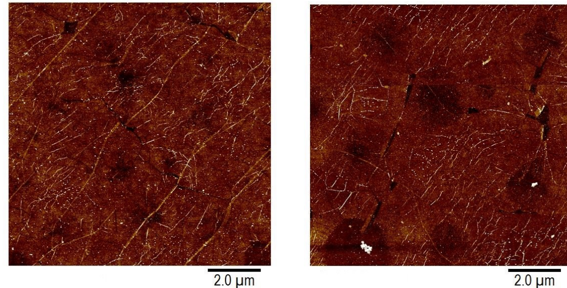

Figure 12: AFM images of CVD graphene transfer with a baking step after transfer to substrate and annealing after acetone bath.

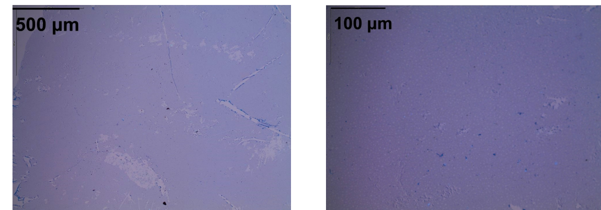

Figure 13: Optical microscope images of CVD graphene transfer with a baking step after transfer to substrate and annealing after acetone bath, with different magnifications.

5.7. Double layer transfer and annealing

A study was carried out on a PMMA CVD graphene transfer batch similar to the standard PMMA transfer, except that, after the first A6 950 K PMMA layer was spin coated (and the polymer was cured in air for 10 minutes), a droplet of A3 950K PMMA was added and cured in air for 2 hours. Thus, after the acetone bath the samples were annealed for 2 hours at 500 °C with a forming gas flow of hydrogen and argon. AFM and optical microscope images obtained from these batches can be seen in figure 14 and 15. The success rate of these transfers was 30%.

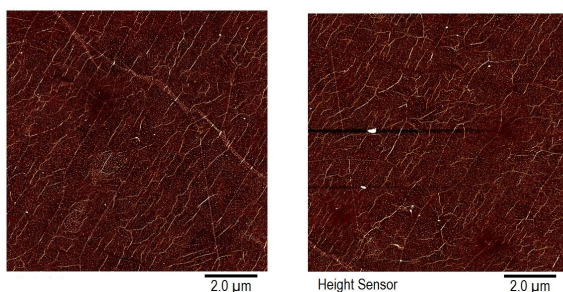

Figure 14: AFM images of CVD graphene transfer carried out with a double PMMA layer and annealing after acetone bath.

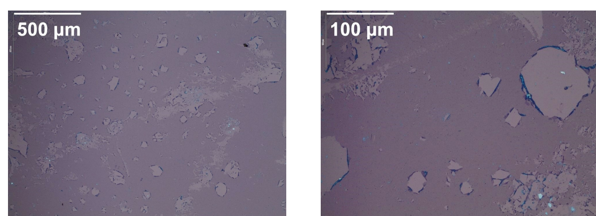

Figure 15: Optical microscope images of CVD graphene transfer carried out with a double PMMA layer and annealing after acetone bath, with different magnifications.

6. Particle and roughness analysis

6.1. AFM and optical images inspection

From the images in figures 2 and 3, the common irregularities associated with CVD graphene transfers can be seen. The white dots shown in the left AFM image, are PMMA residues. The white lines correspond to wrinkles, and can be observed in both images. In the optical microscope images, several tears in the graphene membrane can be observed. Images obtained for the additional HCl cleaning steps, shown in figures 4 and 5, show a reduction in the amount of wrinkles, PMMA residues and breaks in the graphene membrane. On the other hand, addition of a second PMMA layer deteriorated graphene quality by increasing the amount of breaks and tears, as shown in image 7. In the images from figures 8 and 9, that correspond to the experiments with an additional baking step after spin coating, the presence of wrinkles and breaks in the graphene membrane can be observed, however in a smaller quantity, if compared with the images obtained for the standard transfer. Also, it is visible a reduction in the amount of PMMA residues. Addition of a baking step after the transfer lead to rupturing of the graphene membrane, as shown in the images from figures 10 and 11. It can be observed an accumulation of PMMA residues around ruptured area. Comparing images from figures 14 and 15, it can be observed that addition of an annealing step after the acetone bath lead to a reduction of PMMA residues in the sample surface.

6.2. Particle analysis

An analysis was conducted on the particles present in the AFM images, to study the effect of the implemented modifications on PMMA residue density. Particle density for each AFM image was retrieved. Also, particle density average and standard deviation were obtained. In table 1 can be seen the particle density average for each of the modifications on the standard process. Also, with the box plots shown in figure 16, data distribution and the reproducibility of the conducted experiments can be assessed.

	Particle density average (/µm^2)	**Count**
Standard	1,99	5
Extra HCl cleaning	0,44	1
Double layer	1,75	6
Baking after spin coating	1,07	6
Baking after transfer to substrate	0,71	5
Baking after transfer to substrate and annealing	0,23	5
Double layer and annealing	0,58	5

Table 1: Average values obtained for particle density of each image and the number of images used to retrieve the data.

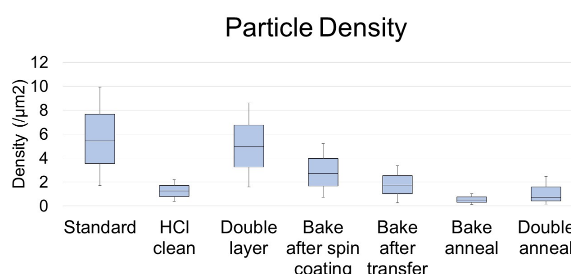

Figure 16: Particle density measurements in AFM images obtained with the standard PMMA transfer and with modifications.

Compared with the standard transfer, the modified HCl cleaning decreased the average particle density by 78%; the double layer transfer by 14%; the

transfer with baking after spin coating by 46% and the baking after transfer to substrate by 65 %. Also, after annealing the samples, the particle density in the transfers with baking step after transfer to substrate, decreased by 78% and, in the double layer transfers, it was reduced by 67%.

Analyzing the plot from figure 16 and the figures obtained for particle density average, it can be verified that both the standard PMMA and the double layer transfer generate the images with the highest density of particles, and produced the most disperse data. Although, with the double layer transfer, particle density average has been reduced by 14%, the amount of micrometer sized tears and ripples is evident, as shown in image 15. Also, since the data retrieved is quite disperse, the results of this experiments are less reproducible, if compared to the experiments carried with other modifications. An increase in PMMA particle density would be expected with the addition of another polymer layer to the copper/graphene/PMMA stack. Baking the films after spin coating also caused a reduction of PMMA residue density since it lead to hardening of the PMMA layer, decreasing the probability of it being destroyed during sample handling while it was still not dry. An additional baking step after the transfer to the substrate lead to a decrease on average particle density. However, it should be remarked that PMMA residues tend to accumulate in irregular areas, suck as breaks or tears of the graphene membrane. For this reason, increasing the duration of HCl cleaning steps lead to a significant decrease in residue density. An efficient removal of wet etchant lead to an improved contact between graphene and substrate, reducing the probability of rupturing the graphene. Annealing the graphene caused the disintegration of PMMA particles due to exposure to high temperatures, leading to a significant decrease in particle density.

6.3. Roughness Analysis

A roughness analysis was conducted on the AFM images to study the effect of the implemented modifications on PMMA residue density. Roughness parameters for each AFM image, and for $1 \times 1 \mu m^2$ sections were retrieved. It was obtained the average and standard deviation for both image and section maximum vertical range (Z range), roughness (Rq) and roughness average (Ra). The average of the roughness parameters, for each of of the modifications is shown in tables 2 and 3. Also, with the box plots shown in figures 17, 18, 19, 20, 21 and 22, data distribution and the reproducibility of the conducted experiments can be assessed.

Image Parameters	Z range (nm)	Rq (nm)	Ra (nm)	Count
Standard	107,27	3,24	1,79	3
Extra HCl cleaning	58,80	1,45	0,84	1
Double layer	80,90	2,59	1,20	6
Baking after spin coating	25,97	0,91	0,50	6
Baking after transfer to substrate	108,42	2,46	0,84	5
Baking after transfer to substrate and annealing	29,50	0,78	0,47	6
Double layer and annealing	58,44	1,46	0,87	5

Table 2: Average values obtained for image maximum vertical range (Z range), roughness (Rq) and roughness average (Ra). Also, the number of samples used in each experiment of this analysis is shown.

Section Parameters	Z range (nm)	Rq (nm)	Ra (nm)	Count
Standard	14,50	1,60	1,20	15
Extra HCl cleaning	9,18	0,90	0,70	5
Double layer	12,34	1,03	0,76	26
Baking after spin coating	5,86	0,44	0,31	24
Baking after transfer to substrate	9,15	1,51	0,69	20
Baking after transfer to substrate and annealing	4,48	0,42	0,34	26
Double layer and annealing	8,90	0,92	0,67	24

Table 3: Average values obtained for maximum vertical range (Z range), roughness (Rq) and roughness average (Ra) for each of the $1 \times 1 \mu m^2$ sections . Also, the number of samples used in each experiment of this analysis is shown.

Image vertical range

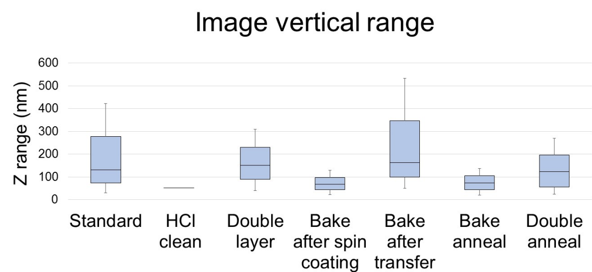

Figure 17: Maximum vertical range measurements in AFM images obtained with the standard PMMA transfer and the modifications.

Compared with the standard transfer, the modified HCl cleaning decreased image average maximum vertical range by 45%; the double layer transfer

by 25%; the transfer with baking after spin coating by 75% and the baking after transfer had no effect on the vertical range. Also, after annealing the samples, the maximum vertical range in the transfers with baking step after transfer to substrate decreased by 73% and in the double layer transfers it was reduced by 77%.

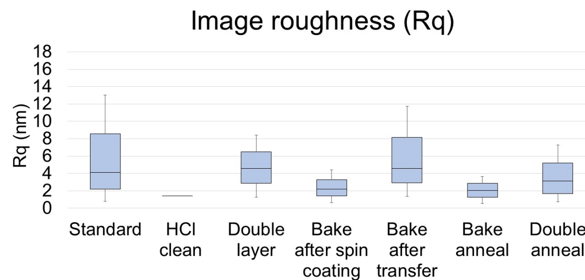

Figure 18: Roughness (Rq) measurements in AFM images obtained with the standard PMMA transfer and the modifications.

Compared with the standard transfer, the modified HCl cleaning decreased the average image roughness (Rq) by 55%; the double layer transfer by 20%; the transfer with baking after spin coating by 70% and the baking after transfer by 73%. Also, after annealing the samples, the maximum vertical range in the transfers with baking step after transfer to substrate decreased by 70% and in the double layer transfers it was reduced by 44%.

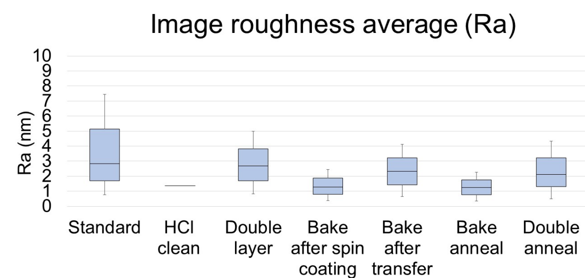

Figure 19: Roughness average (Ra) measurements in AFM images obtained with the standard PMMA transfer and the modifications.

Compared with the standard transfer, the modified HCl cleaning decreased the average image roughness (Ra) 53%; the double layer transfer by 34%; the transfer with baking after spin coating by 25% and the baking after transfer by 72%. Also, after annealing the samples, the maximum vertical range in the transfers with baking step after transfer to substrate decreased by 45% and in the double layer transfers it was reduced by 52%.

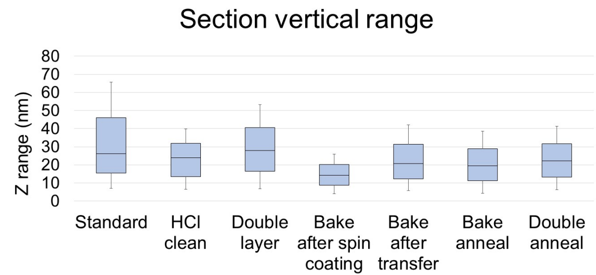

Figure 20: Maximum vertical range measurements in $1 \times 1 \mu m^2$sections of AFM images obtained with the standard PMMA transfer and the modifications.

Compared with the standard transfer, the modified HCl cleaning decreased the section average maximum vertical range by 37%; the double layer transfer by 15%; the transfer with baking after spin coating by 60% and the baking after transfer by 37%. Also, after annealing the samples, the maximum vertical range in the transfers with baking step after transfer to substrate decreased by 48% and in the double layer transfers it was reduced by 28%.

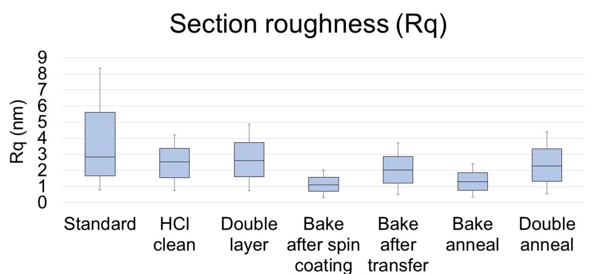

Figure 21: Roughness (Rq) measurements in $1 \times 1 \mu m^2$sections of AFM images obtained with the standard PMMA transfer and the modifications.

Compared with the standard transfer, the modified HCl cleaning decreased the section average image roughness (Rq) 44%; the double layer transfer by 35%; the transfer with baking after spin coating by 73% and the baking after transfer by 5%. Also, after annealing the samples, the maximum vertical range in the transfers with baking step after transfer to substrate decreased by 73% and in the double layer transfers it was reduced by 48%
Compared with the standard transfer, the modified HCl cleaning decreased the section average image roughness (Ra) 42%; the double layer transfer by 37%; the transfer with baking after spin coating by 75% and the baking after transfer by 40%. Also, after annealing the samples, the maximum vertical range in the transfers with baking step after transfer to substrate decreased by 50% and in the double layer transfers, it was reduced by 12%.

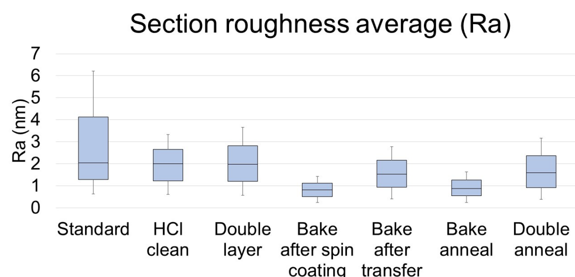

Figure 22: Roughness average (Ra) measurements in $1\times1\mu m^2$sections of AFM images obtained with the standard PMMA transfer and the modifications.

To further understand the effect of the implemented modifications in roughness parameters, data from the entire images (figures: 17, 18, 19) and from sections without PMMA residues or major irregularities (figures: 20, 21 and 22) was retrieved, to assess data uniformity. Data uniformity is altered by irregularities on the sample surface. The data obtained for the entire image varied in a wider range, but is consistent with the values obtained for the selected sections. An experiment with extra cleaning steps was carried out with the goal of improving the cleanliness of the graphene, by removing copper etchant particles that remained attached to the graphene, promoting adhesion of the graphene to the substrate. Although in this experiment the roughness parameters are improved (section parameter improvement varies from 37% to 44%), the success rate was 20% lower than in the standard transfer, because graphene remained in the HCl bath for 20 min, which lead to graphene degradation. Thus, longer DI water cleaning steps lead to improvements. The double layer experiment was carried with the goal of the second PMMA layer diluting the first layer, relaxing it and enhancing contact between graphene and substrate. Although the roughness parameters improve (section parameter improvement varies from 15% to 37%), the success rate was 20% lower than in the standard PMMA transfer. Also, the optical microscope images from figures 7, show increased breaking and rippling of the graphene membrane as shown in the images of figure 15. To harden the PMMA and provide a more efficient graphene support, the PMMA was baked after spin coating. This modification lead to a 40% increase in the success rate and to an 60% to 75% improvement in the section roughness parameters. Also, an experiment was conducted in which the graphene/PMMA films were baked after being transfered, to evaporate any trapped water between graphene and the substrate. If graphene is not properly attached to the substrate, those regions will break, causing tears and ripples when the PMMA is removed. This modification showed an 40% success rate increase and improvements from 5 % to 40 % in section roughness parameters. AFM images from figure 10 and an elevated dispersion of the values obtained for image parameters, as shown in the plots from figures 17 and 18, demonstrate that, despite the improvements on roughness in the section paramenters, which correspond to areas where the graphene appeared intact, this modification lead to breaking of the membrane. Annealing the samples, produced overall improvements, specially on image roughness parameters due to PMMA residues removal, for both experiments conducted.

7. Conclusions

The effect of modifications to the CVD graphene transfer by the PMMA method was studied. Optical and AFM images were retrieved to quantify the effects of the modifications implemented. Particle density and roughness parameters were obtained and a comparative analysis of the data was performed.

Longer HCl cleaning steps enhance the removal of copper etchant residues of the graphene surface. This modification lead to a decrease on residue accumulation and roughness. Optical microscope images showed improvements in rupturing and tearing of graphene membrane. However, only DI water cleaning steps seemed to improve the transfer quality.

Also, the effect of adding a second PMMA layer was studied. Optical images show that the amount of breaking and tearing is significant. However, improvements on PMMA residue accumulation and on roughness parameters were achieved.

Furthermore, an experiment with an additional baking step after spin coating was carried, which showed a significant increase in success rate, section roughness parameters and in particle density. Optical microscope images also showed the formation of wrinkles. An additional baking step was included after the graphene/PMMA films transfer to the substrate. This modification lead to improvements in particle density section roughness parameters and success rate.

Annealing enhances the removal of PMMA residues in the graphene membrane, leading to improvements on particle density and roughness parameters.

References

[1] J. Shendure and H. Ji, “Next-generation DNA sequencing,” *Nature Biotechnology*, vol. 26, pp. 1135–1145, Oct. 2008.

[2] M. Wanunu, “Nanopores : A journey towards DNA sequencing,” *Physics of Life Reviews*, vol. 9, no. 2, pp. 125–158, 2012.

[3] G. F. Schneider, S. W. Kowalczyk, V. E. Calado, G. Pandraud, H. W. Zandbergen, L. M. K. Vandersypen, and C. Dekker, “DNA Translocation through Graphene Nanopores,” *Nano Letters*, vol. 10, no. 8, pp. 3163–3167, 2010.

[4] A. K. Geim and K. S. Novoselov, “The rise of graphene,” *Nature Materials*, vol. 6, pp. 183–191, Mar. 2007.

[5] A. N. Obraztsov, “Chemical vapour deposition: Making graphene on a large scale,” *Nature Nanotechnology*, vol. 4, pp. 212–213, Apr. 2009.

[6] J. Kong, A. M. Cassell, and H. Dai, “Chemical vapor deposition of methane for single-walled carbon nanotubes,” *Chemical Physics Letters*, vol. 292, no. 46, pp. 567 – 574, 1998.

[7] Y. C. Shin, M. S. Dresselhaus, and J. Kong, *Carbon Nanotubes and Graphene*. Elsevier, 2014.

[8] A. Reina, X. Jia, J. Ho, D. Nezich, H. Son, V. Bulovic, M. S. Dresselhaus, and J. Kong, “Large Area, Few-Layer Graphene Films on Arbitrary Substrates by Chemical Vapor Deposition,” *Nano Letters*, vol. 9, no. 1, pp. 30–35, 2009.

[9] G. Varhegyi, M. J. A. Jr., E. Jakab, and P. Szabo, “Kinetic modeling of biomass pyrolysis,” *Journal of Analytical and Applied Pyrolysis*, vol. 42, no. 1, pp. 73 – 87, 1997.

[10] S. Bhaviripudi, X. Jia, M. S. Dresselhaus, and J. Kong, “Role of kinetic factors in chemical vapor deposition synthesis of uniform large area graphene using copper catalyst,” *Nano Letters*, vol. 10, no. 10, pp. 4128–4133, 2010.

[11] L. Vicarelli, S. J. Heerema, C. Dekker, and H. W. Zandbergen, “Controlling Defects in Graphene for Optimizing the Electrical Properties of Graphene Nanodevices,” *ACS Nano*, vol. 9, no. 4, pp. 3428–3435, 2015.

[12] X. Li, C. W. Magnuson, A. Venugopal, J. An, J. W. Suk, B. Han, M. Borysiak, W. Cai, A. Velamakanni, Y. Zhu, L. Fu, E. M. Vogel, E. Voelkl, L. Colombo, and R. S. Ruoff, “Graphene films with large domain size by a two-step chemical vapor deposition process,” *Nano Letters*, vol. 10, no. 11, pp. 4328–4334, 2010.

[13] J. Kang, D. Shin, S. Bae, and B. H. Hong, “Graphene transfer: key for applications,” *Nanoscale*, vol. 4, pp. 5527–5537, 2012.

[14] J. Lee, C. Park, and G. Whitesides, “Solvent Compatibility of Poly(dimethylsiloxane)-Based Microfluidic Devices,” *Analytical Chemistry*, vol. 75, no. 23, pp. 6544–6554, 2003.

[15] K. S. Kim, Y. Zhao, H. Jang, S. Y. Lee, J. M. Kim, K. S. Kim, J.-H. Ahn, P. Kim, J.-Y. Choi, and B. H. Hong, “Large-scale pattern growth of graphene films for stretchable transparent electrodes,” *Nature*, vol. 457, no. 7230, pp. 706–710, 2009.

[16] A. Reina, S. Thiele, X. Jia, S. Bhaviripudi, M. Dresselhaus, J. Schaefer, and J. Kong, “Growth of large-area single- and Bi-layer graphene by controlled carbon precipitation on polycrystalline Ni surfaces,” *Nano Research*, vol. 2, no. 6, pp. 509–516, 2009.

[17] X. Li, W. Cai, J. An, S. Kim, J. Nah, D. Yang, R. Piner, A. Velamakanni, I. Jung, E. Tutuc, S. K. Banerjee, L. Colombo, and R. S. Ruoff, “Large-Area Synthesis of High-Quality and Uniform Graphene Films on Copper Foils,” *Science*, vol. 324, no. 5932, pp. 1312–1314, 2009.

[18] X. Li, Y. Zhu, W. Cai, M. Borysiak, B. Han, D. Chen, R. D. Piner, L. Colombo, and R. S. Ruoff, “Transfer of Large-Area Graphene Films for High-Performance Transparent Conductive Electrodes,” *Nano Letters*, vol. 9, no. 12, pp. 4359–4363, 2009.

[19] A. Pirkle, J. Chan, A. Venugopal, D. Hinojos, C. W. Magnuson, S. McDonnell, L. Colombo, E. M. Vogel, R. S. Ruoff, and R. M. Wallace, “The effect of chemical residues on the physical and electrical properties of chemical vapor deposited graphene transferred to SiO2,” *Applied Physics Letters*, vol. 99, no. 12, 2011.

[20] W.-H. Lin, T.-H. Chen, J.-K. Chang, J.-I. Taur, Y.-Y. Lo, W.-L. Lee, C.-S. Chang, W.-B. Su, and C.-I. Wu, “A Direct and Polymer-Free Method for Transferring Graphene Grown by Chemical Vapor Deposition to Any Substrate,” *ACS Nano*, vol. 8, no. 2, pp. 1784–1791, 2014.